Iranian Society of Acoustics and Vibration
The 14th ISAV2024 International Conference on Acoustics and Vibration
11-12 Dec 2024 Karaj - Iran
Kharazmi University

Investigating Stiffeners Influence on Stability of Axially -Compressed Metamaterial Sandwich Toroidal Shells Containing Graphene Origami-Enabled Auxetic Core (ISAV2024)

Mohammadhossein Goudarzfallahi[b], Ali Alinia Ziazi[b], Farzad Ebrahimi[a*]

[a] *Department of Mechanical Engineering, Faculty of Engineering, Imam Khomeini International University, Qazvin, Iran*

[b] *Mechanical Engineering Department, Science and Research branch, Islamic Azad University, Tehran, Iran*

** Corresponding author e-mail: febrahimy@eng.ikiu.ac.ir*

Abstract

This study examines the buckling and post-buckling behavior of stiffened sandwich toroidal shell segments (TSSs) with a graphene origami (GOri)-enabled auxetic core and carbon nanotube (CNT)-reinforced face sheets supported by elastic foundations under axial compression. The TSSs are stiffened with CNT-reinforced stringers or rings, modeled using a novel smeared stiffener technique. CNTs are distributed uniformly (UD) or functionally graded (FG) across the face sheets and stiffeners. Nonlinear equilibrium equations are derived using von Kármán shell theory and Stein and McElman approximations, with a Winkler-Pasternak elastic foundation considered for shell-foundation interactions. The Galerkin method is used to solve the nonlinear load-deflection relationship, which is then applied to calculate buckling loads and analyze post-buckling behavior. Numerical investigations focus on the effects of stiffeners, CNT volume fraction, and distribution types on the buckling and post-buckling behavior of auxetic-core TSSs, confirming that stiffeners substantially enhance the critical buckling loads and post-buckling strength.

Keywords: stiffeners; auxetic core; buckling and post-buckling; toroidal shells

1. Introduction

As auxetic metamaterials attract significant attention across various industries due to their excellent mechanical properties, extensive research has focused on developing materials that combine auxeticity with strong mechanical performance over the past few decades [1]. Recently, a category of graphene origami (GOri)-enabled metallic metamaterials (GOEAMs) with superior mechanical properties has been developed by Zhao et al. [2]. These materials offer tunable negative Poisson's ratio (NPR) and enhanced mechanical properties, with NPR adjustability achievable by altering the graphene content, folding degree, and temperature. Ebrahimi and Parsi [3] studied wave propagation in auxetic beams with FG GOri. Ebrahimi and Ahari [4] examined buckling in composite materials with magnetostrictive face sheets and GOri features.

Carbon nanotubes (CNTs) are ideal for enhancing composites due to their exceptional thermal, mechanical, and electrical properties [5]. CNTs can be uniformly distributed (UD) or functionally graded (FG) within a polymer matrix when incorporated as fibers. Using a perturbation technique, Shen [6] analyzed post-buckling in FG-CNTRC cylindrical shells. Shen [7] also examined post-buckling in CNT-reinforced cylindrical shells under axial loading in a thermal environment using higher-order shear deformation theory.

Toroidal shell segments (TSSs) are widely used in engineering applications, including aeronautical, underwater, and civil structures. Recent research has focused on the buckling analysis of these shells, particularly those made from modern composite materials. Nguyen et al. [8] analyzed buckling and post-buckling in TSSs with honeycomb auxetic cores and GRC coatings under torsional loads, using von Karman-Donnell shell theory and Stein and McElman approximations [9] with the Galerkin method. Ebrahimi et al. [10] found that sandwich TSSs with GOREAM cores and CNTRC face sheets had significantly better stability than those with re-entrant auxetic metamaterials. Multiple studies have been undertaken using a similar approach to analyze the buckling and post-buckling behavior of TSSs [11–14].

Optimally designed stiffeners enhance shell structure buckling behavior. Wang et al. [15] introduced a smeared stiffener method for stiffened composite shells, later improved by Phuong et al. [16] for FG-GRC shells' nonlinear and post-buckling analysis. Dong et al. [17] studied nonlinear buckling in CNTRC shells with CNTR stiffeners. Dao et al. [18] analyzed buckling in eccentrically stiffened FG TSSs, while Minh et al. [19] applied Phuong et al.'s method to CNTRC TSSs with FG-CNTRC stiffeners.

A comprehensive literature review on TSSs highlights a significant gap in understanding how stiffeners affect the buckling and post-buckling behavior of sandwich composite auxetic-core TSSs. To address this, the authors propose investigating TSSs with a GOEAM core and CNT-reinforced coatings using Phuong et al.'s [16] smeared stiffener technique. The study, focusing on axial compression with Pasternak's elastic foundations, integrates von Kármán nonlinearity with the Stein and McElman approximation and uses the Galerkin method for analysis. It conducts a parametric study to examine the effects of various stiffener types and CNT parameters.

2. Geometrical and material description

2.1 The CNT-reinforced face sheet-stiffener structure

Figure 1 shows the geometry of ring- and stringer-stiffened auxetic-core sandwich TSSs. This study models the shell-stiffener structure using an improved smeared stiffener technique [16]. FG-CNTRC stiffeners maintain consistent CNT orientation across the face sheets and stiffeners with patterns similar to the shell—UD, FG-X, and FG-O. The extended rule of mixture determines the elastic constants of orthotropic materials as follows [6]:

$$E_{11}^{CNTRC} = V_{ma}E_{ma} + \eta_1 V_{CNT}E_{11}^{CNT} \qquad \nu_{12}^{CNTRC} = V_{ma}\nu_{ma} + V_{CNT}\nu_{12}^{CNTR}$$

$$E_{22}^{CNTRC} = \frac{\eta_2}{\frac{V_{CNT}}{E_{22}^{CNT}} + \frac{V_{ma}}{E_{ma}}} \qquad G_{12}^{CNTRC} = \frac{\eta_3}{\frac{V_{CNT}}{G_{12}^{CNT}} + \frac{V_{ma}}{G_{ma}}} \tag{1}$$

here $E_{11}^{\mathrm{CNT}}, E_{22}^{\mathrm{CNT}}$, and G_{12}^{CNT}represent the elastic moduli for the CNTs, while E_{ma} and G_{ma}denote the elastic moduli of the matrix material. η_j signifies the performance parameter, and V_{CNT} and V_{ma} are the volume fractions of the CNTs and the matrix, respectively, with $V_{\mathrm{CNT}} + V_{ma} = 1$. Furthermore. Poisson's ratios are ν_{12}^{CNT} and ν_{ma} for CNTs and matrix materials, respectively.

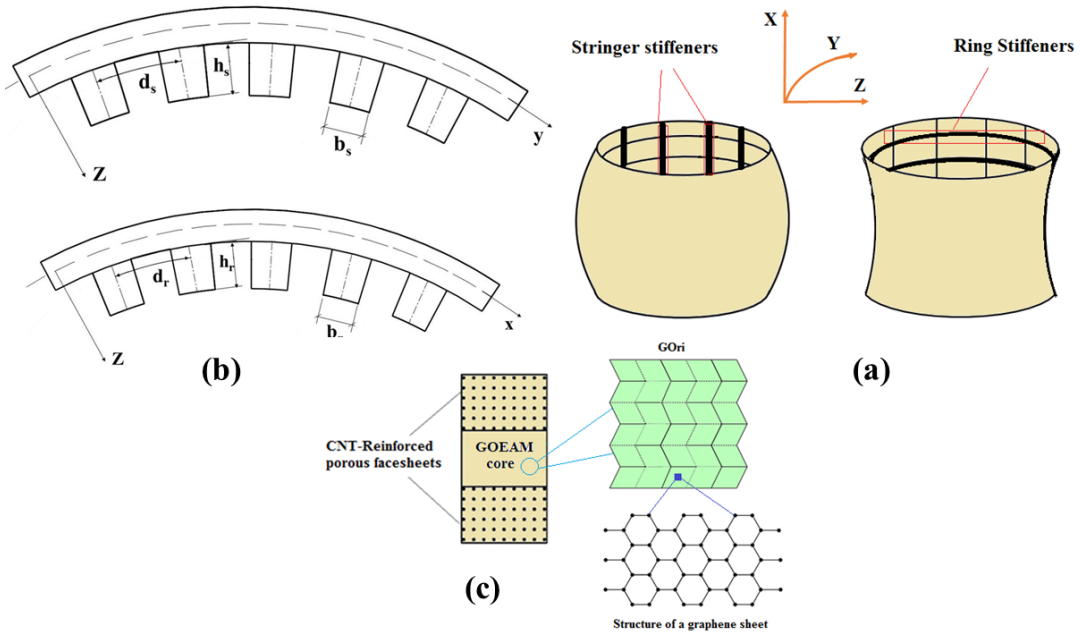

Figure 1. Configuration of stiffened sandwich GOEAM -core TSSs with CNTRC shell-stiffener structure.

2.2 Effective mechanical properties of GOEAM core

The mechanical properties of GOEAM, including Young's modulus E_c, Poisson's ratio ν_c, coefficient of thermal expansion α_c, and density ρ_c, as developed by Zhao et al. [2], can be expressed as follows:

$$E_c = \frac{1+\xi\eta\, V_{Gr}}{1-\eta V_{Gr}} E_{Cu} \times f_E(H_{Gr}, V_{Gr}, T) \qquad \nu_c = (\nu_{Gr}V_{Gr} + \nu_{Cu}V_{Cu}) \times f_\nu(H_{Gr}, V_{Gr}, T)$$
$$\alpha_c = (\alpha_{Gr}V_{Gr} + \alpha_{Cu}V_{Cu}) \times f_\alpha(V_{Gr}, T) \qquad \rho_c = (\rho_{Gr}V_{Gr} + \rho_{Cu}V_{Cu}) \times f_\rho(V_{Gr}, T) \tag{2}$$

where η and ξ are material and size coefficients from Zhao et al. [2], and T is 300 K.

3. Fundamental equations

This paper uses von Karman-Donnell's theory to derive the governing equations for the buckling and post-buckling characteristics of stiffened sandwich TSSs with GOEAM cores and CNT-reinforced face sheets under uniform axial compression. According to Stein and McElman [9], the mid-surface strain of the shells is as follows:

$$\varepsilon_x^0 = \frac{\partial u}{\partial x} + \left(\frac{\partial w}{\partial x}\right)^2 - \frac{w}{a}$$
$$\varepsilon_y^0 = \frac{\partial v}{\partial x} + \left(\frac{\partial w}{\partial y}\right)^2 - \frac{w}{R} \tag{3}$$
$$\gamma_{xy}^0 = \frac{\partial u}{\partial y} + \frac{\partial v}{\partial x} + \frac{\partial w}{\partial x}\frac{\partial w}{\partial y}$$

where u, v and w, are displacement components in the x, y and z directions, respectively Hooke's law is utilized for orthotropic layers, as [20]:

$$\begin{bmatrix}\sigma_x\\ \sigma_y\\ \sigma_{xy}\end{bmatrix}=\begin{bmatrix}Q_{11} & Q_{12} & 0\\ Q_{12} & Q_{22} & 0\\ 0 & 0 & Q_{66}\end{bmatrix}\begin{bmatrix}\varepsilon_x\\ \varepsilon_y\\ \gamma_{xy}\end{bmatrix} \tag{4}$$

where

$$Q_{11}=\frac{E_{11}}{1-\nu_{12}\nu_{21}} \qquad Q_{12}=\frac{E_{11}\nu_{21}}{1-\nu_{12}\nu_{21}} \quad Q_{22}=\frac{E_{22}}{1-\nu_{12}\nu_{21}} \qquad Q_{66}=G_{12} \tag{5}$$

Integrating Eq. (4) across the shell and stiffener thickness allows derivation of the internal forces in stiffened sandwich TSSs as follows:

$$\begin{bmatrix}N_x\\ N_y\\ N_{xy}\\ M_x\\ M_y\\ M_{xy}\end{bmatrix}=\begin{bmatrix}A_{11} & A_{12} & 0 & B_{11} & B_{12} & 0\\ A_{12} & A_{22} & 0 & B_{12} & B_{22} & 0\\ 0 & 0 & A_{66} & 0 & 0 & B_{66}\\ B_{11} & B_{12} & 0 & D_{11} & D_{12} & 0\\ B_{12} & B_{22} & 0 & D_{12} & D_{22} & 0\\ 0 & 0 & B_{66} & 0 & 0 & D_{66}\end{bmatrix}\begin{bmatrix}\varepsilon_x^0\\ \varepsilon_y^0\\ \gamma_{xy}^0\\ -w_{,xx}\\ -w_{,yy}\\ -2w_{,xy}\end{bmatrix} \tag{6}$$

Where $A_{ij}, B_{ij},$ and D_{ij} are the total stiffnesses of the stiffened sandwich TSSs, expressed as [16]:

$$\left(A_{ij}, B_{ij}, D_{ij}\right)=\left(A_{ij}^{sh}, B_{ij}^{sh}, D_{ij}^{sh}\right)+\left(A_{ij}^{s}, B_{ij}^{s}, D_{ij}^{s}\right)+\left(A_{ij}^{r}, B_{ij}^{r}, D_{ij}^{r}\right) \quad (i,j=1,2,6) \tag{7}$$

where $A_{ij}^{sh}, B_{ij}^{sh}, D_{ij}^{sh}$ represent the sandwich shell's stiffness .The stiffness of CNTR ring can be obtained by using the expression [16]:

$$\begin{bmatrix}A_{22}^{r} & B_{22}^{r}\\ B_{22}^{r} & D_{22}^{r}\end{bmatrix}=\begin{bmatrix}\tilde{A}_{22} & \tilde{B}_{22}\\ \tilde{B}_{22} & \tilde{D}_{22}\end{bmatrix}-\begin{bmatrix}\tilde{A}_{12} & 0 & \tilde{B}_{12} & 0\\ \tilde{B}_{12} & 0 & \tilde{D}_{12} & 0\end{bmatrix}\begin{bmatrix}\tilde{A}_{11} & 0 & \tilde{B}_{11} & 0\\ 0 & \tilde{A}_{66} & 0 & \tilde{B}_{66}\\ \tilde{B}_{11} & 0 & \tilde{D}_{11} & 0\\ 0 & \tilde{B}_{66} & 0 & \tilde{D}_{66}\end{bmatrix}\begin{bmatrix}\tilde{A}_{12} & \tilde{B}_{12}\\ 0 & 0\\ \tilde{B}_{12} & \tilde{D}_{12}\\ 0 & 0\end{bmatrix} \tag{8}$$

where

$$\left(\tilde{A}_{ij}, \tilde{B}_{ij}, \tilde{C}_{ij}\right)=\frac{b_r}{d_r}\int_{\Omega_r}\tilde{Q}_{ij}\,(1, z, z^2)dz \qquad (i,j=1,2,6) \tag{9}$$

The same calculation procedure applies to stringers. The equilibrium equations for stiffened sandwich TSSs, are expressed as follows [14]

$$\begin{gathered}N_{x,x}+N_{xy,y}=0\\ N_{xy,x}+N_{y,y}=0\\ M_{x,xx}+M_{y,yy}+2M_{xy,xy}+N_xw_{,xx}+N_yw_{,yy}+2N_{xy}w_{,xy}+\frac{N_x}{a}+\frac{N_y}{R}\\ -K_1w+K_2\left(w_{,xx}+w_{,yy}\right)=0\end{gathered} \tag{10}$$

The Airy stress function $\varsigma(x,y)$ may be introduced as:

$$\phi_{,yy}=N_x,\ \phi_{,xx}=N_y,\ \phi_{,xy}=-N_{xy} \tag{11}$$

When conditions (11) are met, the first two equations in Eq. (10) are satisfied. Substituting Eq. (6) and Eq. (11) into the last equation of Eq. (10) yields the equilibrium equations as follows:

$$\begin{gathered}D_{11}w_{,xxxx}+D_{22}w_{,yyyy}+(D_{12}+D_{21}+4D_{66})w_{,xxyy}-\frac{1}{R}\phi_{,xx}-\frac{1}{a}\phi_{,yy}\\ -\phi_{,yy}w_{,xx}-\phi_{,xx}w_{,yy}+2\phi_{,xy}w_{,xy}+K_1w-K_2\left(w_{,xx}+w_{,yy}\right)=0\end{gathered} \tag{12}$$

From Eq. (3) the deformation compatibility equation is obtained as:

$$\varepsilon_{x,yy}^0+\varepsilon_{y,xx}^0-\gamma_{xy,xy}^0+\frac{1}{R}w_{,xx}+\frac{1}{a}w_{,yy}-w_{,xy}^2+w_{,xx}w_{,yy}=0 \tag{13}$$

Substituting Eq. (6) into the compatibility Eq. (12) yields:

$$\bar{C}_{11}\,\phi_{,xxxx} + \bar{C}_{22}\,\phi_{,yyyy} + (\bar{C}_{66} - 2\bar{AC}_{12})\,\phi_{,xxyy} - w_{,xy}^2 + w_{,xx}w_{,yy} + \frac{1}{R}w_{,xx} + \frac{1}{a}w_{,yy} = 0 \tag{14}$$

Applying the closed condition to the closed shell yields:

$$\int_0^{2\pi R}\int_0^{L} v_{,y}dxdy = \int_0^{2\pi R}\int_0^{L}\left(\varepsilon_y^0 + \frac{w}{R} - \frac{1}{2}w_{,y}^2\right)dxdy = 0 \tag{15}$$

The governing Eqs. (16, 18, 19) can be utilized to explore the post-buckling behavior of sandwich TSSs.

4. Solution Procedure

This article examines the buckling and post-buckling analysis of stiffened axially-loaded sandwich TSSs considering simply-supported boundary conditions as follows:

$$w = 0, N_x = 0, N_{xy} = 0, M_x = 0 \qquad x=0, x=L \tag{16}$$

In accordance with the boundary condition the deflection of the shell $w(x, y)$ can be approximated by a three-term expression as [14]

$$w = \xi_0 + \xi_1 \sin\frac{m\pi x}{L}\sin\frac{ny}{R} + \xi_2 \sin^2\frac{m\pi x}{L} \tag{17}$$

where *m* and *n* are the longitudinal and radial buckling modes, ξ_0 is the pre-buckling deflection amplitude, and ξ_1, ξ_2 are the linear and nonlinear post-buckling deflection amplitudes. Substituting Eq. (17) into (14) yields the stress function:

$$\phi = \phi_1 \cos\frac{2m\pi x}{L} + \phi_2 \cos\frac{2ny}{R} - \phi_3 \sin\frac{m\pi x}{L}\sin\frac{ny}{R} + \phi_4 \sin\frac{3m\pi x}{L}\sin\frac{ny}{R} - \sigma_{0y}h\frac{x^2}{2} - p_0 h\frac{y^2}{2} \tag{18}$$

Where p_0 is the compressive axial load, and the ϕ_i are provided in [14]. By substituting the stress function (18) and deflection Eq. (17) in equation (12), applying the Galerkin method, and considering the Eq. (15), the equilibrium equations are derived as follows:

$$\nu_0 = \frac{S_{32}}{2S_{31}}\nu_1^2 - \frac{\nu_2}{2} - \frac{S_{34}}{2S_{31}}p_0 \tag{19}$$

$$S_{11} + S_{12}\nu_0 + S_{13}\nu_1^2 + S_{14}\nu_2 + S_{15}\nu_2^2 - S_{16}p_0 = 0 \tag{20}$$

$$\nu_1^2 = \frac{-S_{23}\nu_2 + S_{24}\nu_2 p_0}{S_{21} + S_{22}\nu_2} \tag{21}$$

where S_{ij} are presented in [14]. By solving Eqs. (19)– (21), the load expression in terms of the nonlinear amplitude can be obtained as follows:

$$\begin{aligned} p_0 = &\left[S_{11} + \left(S_{14} - \frac{S_{12}}{2}\right)\nu_2 + S_{15}\nu_2^2 - \frac{S_{12}S_{23}S_{32}\nu_2}{2S_{31}(S_{21} + S_{22}\nu_2)} - \frac{S_{13}S_{23}\nu_2}{S_{21} + S_{22}\nu_2}\right] \\ &\times\left(S_{16} + \frac{S_{12}S_{34}}{2S_{31}} - \frac{S_{13}S_{24}\nu_2}{S_{21} + S_{22}\nu_2} - \frac{S_{12}S_{24}S_{32}\nu_2}{2S_{31}(S_{21} + S_{22}\nu_2)}\right)^{-1} \end{aligned} \tag{22}$$

Setting $\nu_2 = 0$ allows the determination of the bifurcation point for the upper buckling load of axially compressed TSSs.

$$p_0^{upper} = S_{11}/[S_{16} - S_{12}S_{34}/(2S_{31})] \tag{23}$$

From Eqs. (19) -(21), one can establish the relationship between maximum deflection and nonlinear amplitude.

$$w_{\max} = \frac{S_{32}(S_{24}\nu_2 p_0 - S_{23}\nu_2)}{2S_{31}(S_{21} + S_{22}\nu_2)} + \frac{\nu_2}{2} + \left(\frac{S_{24}\nu_2 p_0 - S_{23}\nu_2}{S_{21} + S_{22}\nu_2}\right) - p_0\frac{S_{34}}{2S_{31}} \tag{24}$$

The post-buckling curves $p_0 - W_{\max}/h$ of stiffened GOEAM-core sandwich TSSs with CNT-reinforced face sheets can be obtained by combining Eqs. (22) and (24).

5. Numerical Results and Discussion

To validate the method used in this investigation, comparative studies were conducted on a CNT-reinforced cylindrical shell without stiffeners, assuming an infinite longitudinal radius and no elastic foundation. The critical buckling loads from this study show acceptable agreement with those reported by Shen et al. [9], as indicated in Table 1.

Table 1. Comparisons of critical buckling load $\bar{p}_{cr} = p_{cr}2\pi Rh$(in KN) of CNTRC cylindrical shells subjected to axial compression *(R/h* = 100 , *h* = 1 mm , $h_2 = 0$, *T* = 300 K).

L^2/Rh	V_{CNT}	Shen [9]		Present	
		UD	FG-X	UD	FG-X
	0.12	18.75 (1,7)*	21.81 (1;7)	18.8321 (1,7)	21.638 (1,7)
100	0.17	30.43 (1,7)	35.53 (1;7)	30.5419 (1,7)	35.2354 (1,7)
	0.28	37.77 (1,7)	47.18 (1;7)	38.0149 (1,7)	47.2022

*The buckling modes are represented as (*m*,*n*)

Tables 2–3. detail the impact of CNTR rings, stringers, CNT reinforcement direction, distribution patterns, and content on the critical buckling loads of TSSs. The results show that FG-CNTRC convex TSSs have higher critical buckling loads than concave ones. For convex TSSs, longitudinal CNT reinforcement yields greater buckling loads, while concave shells perform better with circumferential reinforcement. Tables 2. and 3 also reveal that the FG-X CNTRC distribution pattern achieves the highest buckling loads, whereas the FG-O pattern results in the lowest. Stiffeners are crucial: unstiffened TSSs have significantly lower buckling loads than stiffened shells. For convex TSSs, stringer-stiffened shells outperform ring-stiffened ones, whereas, for concave TSSs, ring-stiffened shells are more effective. In all cases, increasing CNT content markedly enhances buckling loads.

Table 2. The critical buckling loads (in MPa) of GOri-enabled sandwich convex TSSs with and without CNTRC stiffeners subjected to axial compression. (*H_{Gr} = 100%, W_{Gr} = 2.5%, L = 1.5R, R/h = 80, a=4R* $,h_1 = 1mm,h_2 = 2mm,\ b_s = b_r = 0.002\ m, h_s = h_r = 0.003m,\ n_s = 50, n_r = 12$*)*

		XD TSS				YD TSS		
	V_{CNT}	Without stiffener	XD stiffeners	YD stiffeners		Unstiffened	XD stiffeners	YD stiffeners
UD	**0.17**	550.03 (6,5)	612.415 (5,6)	557.163 (6,6)		300.703 (12,6)	472.946 (7,8)	302.09 (12,7)
	0.28	678.622 (5,5)	778.771 (5,5)	688.292 (5,6)		346.978 (12,7)	580.284 (7,8)	347.537 (12,7)
	0.17	593.942 (5,6)	654.755 (5,6)	598.962 (5,6)		303.79 (12,6)	485.355 (7,8)	305.335 (12,6)
	0.28	743.193 (5,5)	832.76 (4,6)	755.068 (5,6)		355.929 (12,7)	602.27 (7,8)	356.608 (12,7)
	0.17	495.669 (6,5)	570.753 (5,6)	501.581 (6,6)		299.136 (12,6)	461.507 (7,8)	299.826 (12,7)
	0.28	616.525 (5,6)	713.154 (5,5)	623.906 (5,6)		343.152 (12,8)	561.669 (6,8)	343.42 (12,8)

Table 3. The critical buckling loads (in MPa) of GOri-enabled sandwich concave TSSs with and without CNTR stiffeners subjected to axial compression. (*H_{Gr} = 100%, W_{Gr} = 2.5%, L = 1.5R, R/h = 80, a=-4R* $,h_1 = 1mm,h_2 = 2mm,\ b_s = b_r = 0.002\ m, h_s = h_r = 0.003m,\ n_s = 50, n_r = 12$*)*

		XD TSS				YD TSS		
	V_{CNT}	Unstiffened	XD stiffeners	YD stiffeners		Unstiffened	XD stiffeners	YD stiffeners
FG-X	**0.12**	105.388 (1,4)	106.015 (1,4)	117.36 (1,4)		140.534 (1,4)	141.017 (1,4)	153.626 (1,4)
	0.17	108.186 (1,4)	109.153 (1,4)	125.138 (1,4)		159.328 (1,4)	160.029 (1,4)	178.436 (1,4)
	0.28	111.921 (1,4)	113.623 (1,4)	137.939 (1,4)		195.979 (1,4)	197.099 (1,4)	227.08 (1,4)

Figures 4a and 4b analyze the effects of stiffeners on the post-buckling curves of sandwich TSSs, comparing stiffened and unstiffened shells for convex and concave TSSs with longitudinal and circumferential CNT-reinforced shell structures. Stiffeners significantly impact post-buckling behavior. For convex TSSs, Figure 4a shows that stringer-type stiffeners yield higher post-buckling curves, while for concave TSSs, ring-stiffened shells exhibit the highest curves (Figure 4b). Additionally, Figure 4 highlights the complexity of TSS nonlinear behavior, with convex TSSs showing irregular

post-buckling paths due to material and geometric complexities, especially at higher deflections, complicating the prediction of their behavior. Figures 6a and 6b show the effect of CNT distribution patterns—UD, FG-X, and FG-O—on stiffened TSSs' post-buckling behavior. FG-X offers the best strength, followed by UD, with FG-O performing the weakest. Snap-through is minimal in concave TSSs and absent in convex shells.

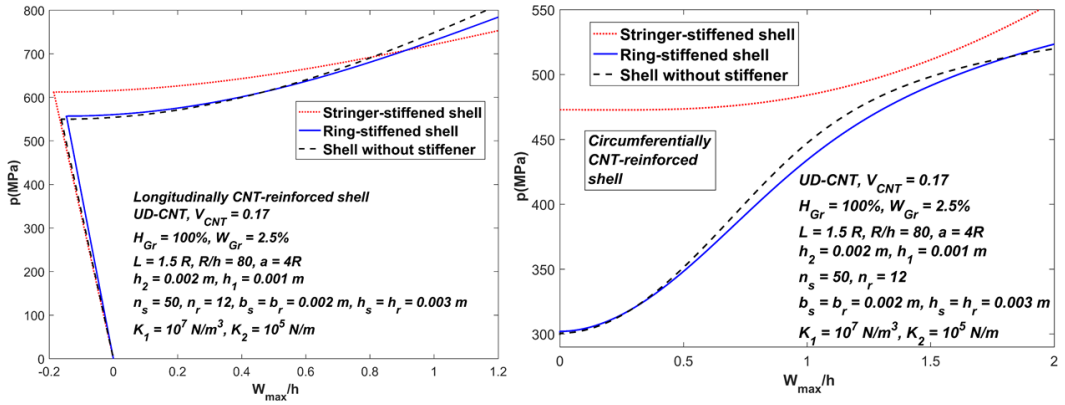

Figure 4. Comparison of stiffener types on the post-buckling curves of convex TSSs with **a**: longitudinal CNT reinforcement **and b**: circumferential CNT reinforcement.

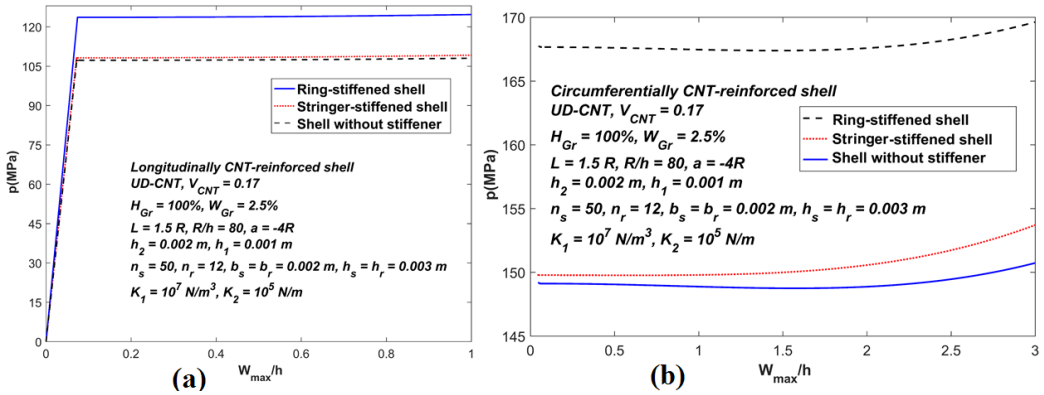

Figure 5. Comparison of stiffener types on the post-buckling curves of concave TSSs with **a**: longitudinal CNT reinforcement **and b:** circumferential CNT reinforcement.

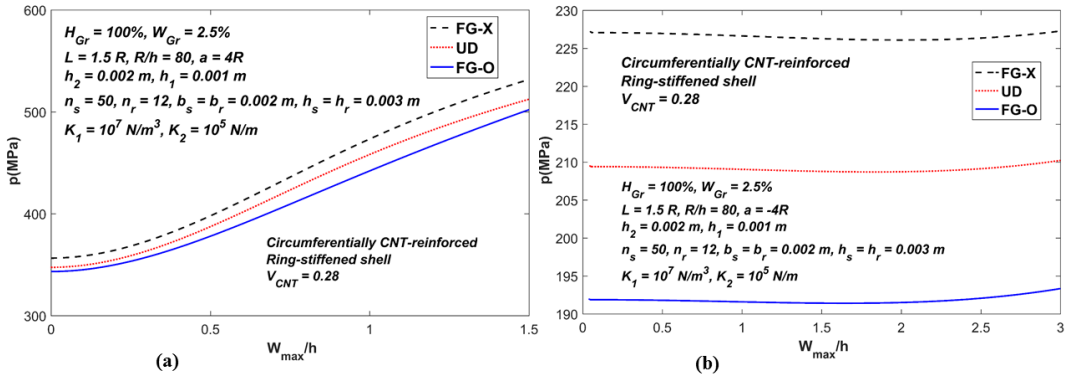

Figure 6. Effects of different CNT distribution models on the post-buckling curves of stiffened TSSs

6. Conclusions

This paper examines the buckling and post-buckling behavior of stiffened GOEAM-core sandwich TSSs with CNT-reinforced face sheets under axial compression, using the Donnell-von Kármán theory, an improved smeared stiffener method, and the Galerkin solution. Numerical studies confirm

that stiffened TSSs exhibit higher critical buckling loads and post-buckling strength than unstiffened shells. Stiffened convex TSSs outperform stiffened concave TSSs in buckling loads and post-buckling strength. The type of stiffeners and CNT reinforcement direction significantly affect the buckling behavior, with longitudinally aligned CNTs and stringer stiffeners boosting performance in convex TSSs and circumferentially reinforced ring stiffeners enhancing performance in concave TSSs. The FG-X CNT distribution pattern yields the best buckling and post-buckling characteristics.

REFERENCES

1. Ebrahimi, F. (2024). *Mechanics of Auxetic Materials and Structures*. CRC Press.
2. Zhao, S., Zhang, Y., Zhang, Y., Zhang, W., Yang, J., & Kitipornchai, S. (2022). Genetic programming-assisted micromechanical models of graphene origami-enabled metal metamaterials. *Acta Materialia*, **228**, 117791.
3. Ebrahimi, F., & Parsi, M. (2023). Wave propagation analysis of functionally graded graphene origami-enabled auxetic metamaterial beams resting on an elastic foundation. *Acta Mechanica*, **234**(12), 6169-6190.
4. Ebrahimi, F., & Ahari, M. F. (2024). On the buckling of meta-graphene-origami-enabled magnetostrictive nanoplates under temperature gradient. *Acta Mech* **235**, 2611–2628.
5. Ebrahimi, F., & Dabbagh, A. (2022). *Mechanics of multiscale hybrid nanocomposites*. Elsevier.
6. Shen, H. S. (2014). Torsional postbuckling of nanotube-reinforced composite cylindrical shells in thermal environments. *Composite Structures*, **116**, 477-488.
7. Shen, H. S. (2011). Postbuckling of nanotube-reinforced composite cylindrical shells in thermal environments, Part I: Axially-loaded shells. Composite Structures, **93**(8), 2096-2108.
8. Nguyen, T. P., Vu, M. D., Dang, T. D., Cao, V. D., Pham, T. H., & Vu, H. N. (2023). An analytical approach of nonlinear buckling behavior of torsionally loaded auxetic core toroidal shell segments with graphene reinforced polymer coatings. *Advanced Composite Materials***,** **32**(3), 400-418.
9. Stein, M., & McElman, J. A. (1965). Buckling of segments of toroidal shells. *AIAA Journal*, *3*(9), 1704-1709.
10. Ebrahimi, F., Goudarzfallahi, M., & Ziazi, A. A. (2024). Static stability analysis of graphene origami-reinforced nanocomposite toroidal shells with various auxetic cores. *Advances in Nano Research*, **17**(1), 1.
11. Van Tien, N., Duc, V. M., Nam, V. H., Phuong, N. T., Ho, L. S., Dong, D. T., . & Minh, T. Q. (2022). Nonlinear postbuckling of auxetic-core sandwich toroidal shell segments with CNT-reinforced face sheets under external pressure. *International Journal of Structural Stability and Dynamics*, **22**(01), 2250006.
12. Phuong, N. T., Van Doan, C., Duc, V. M., Giang, N. T., & Nam, V. H. (2023). Analytical solution for nonlinear buckling of convex and concave auxetic-core toroidal shell segments with graphene-reinforced face sheets subjected to radial loads. *Archive of Applied Mechanics*, **93**(2), 621-634.
13. Hieu, P. T., & Tung, H. V. (2020). Postbuckling behavior of carbon-nanotube-reinforced composite toroidal shell segments subjected to thermomechanical loadings. *AIAA Journal*, **58**(7), 3187-3198.
14. Nam, V. H., Duc, V. M., Doan, C. V., Xuan, N. T., & Phuong, N. T. (2022). Nonlinear postbuckling behavior of auxetic-core toroidal shell segments with Graphene reinforced face sheets under axial loads. *Archives of Mechanics*, **74** *(2-3), 89-108*
15. Wang, B., Tian, K., Hao, P., Zheng, Y., Ma, Y., & Wang, J. (2016). Numerical-based smeared stiffener method for global buckling analysis of grid-stiffened composite cylindrical shells. *Composite Structures*, **152**, 807-815.
16. Phuong, N. T., Trung, N. T., Van Doan, C., Thang, N. D., Duc, V. M., & Nam, V. H. (2020). Nonlinear thermomechanical buckling of FG-GRC laminated cylindrical shells stiffened by FG-GRC stiffeners subjected to external pressure. *Acta Mechanica*, **231**(12), 5125-5144.
17. Dong, D. T., Hieu, P. T., Duc, V. M., Phuong, N. T., Tien, N. V., & Nam, V. H. (2023). Nonlinear Buckling Analysis of Stiffened Carbon Nanotube-Reinforced Cylindrical Shells Subjected to External Pressure in Thermal Environment. *Mechanics of Composite Materials*, **59**(4), 779-794.
18. Dao, B. H., Dinh, N. G., & Tran, T. I. (2016). Buckling analysis of eccentrically stiffened functionally graded toroidal shell segments under mechanical load. *Journal of Engineering Mechanics*, **142**(1), 04015054.
19. Minh, T. Q., Duc, V. M., & Phuong, N. T. (2022). Nonlinear Buckling Behavior of FG-CNTRC Toroidal Shell Segments Stiffened by FG-CNTRC Stiffeners Under External Pressure. In *Modern Mechanics and Applications: Select Proceedings of ICOMMA 2020* (pp. 240-255). Springer Singapore.
20. Reddy, J. N., & Starnes Jr, J. H. (1993). General buckling of stiffened circular cylindrical shells according to a layerwise theory. *Computers & Structures*, **49**(4), 605-616.